Chapter 10

# Optical Techniques for Defect Evaluation in Vehicles

J. P. Carmo and J. E. Ribeiro

Additional information is available at the end of the chapter

http://dx.doi.org/10.5772/46108

## 1. Introduction

The optical techniques are a powerful tool on situations where either the physical contact or invasive techniques for evaluation are not suitable. Vehicle environments constitute an application field for the optical techniques and are the focus of this chapter. In order to reinforce this kind of techniques, it must be clarified that the idea to manipulate the light backs to the second century before our age, when Archimedes planned to destroy enemy ships using a solar heat ray with an array of actuators to change the shape of a mirror (Bifano T., 2011). Therefore, the field of photonics is the one that offers the possibility to achieve one of the greatest realizations and applications because the light is present in all aspects of the human life and our way of living is impossible without light (Carmo J. P. *et al*., 2012a). Optical measurement systems are also suitable for harsh monitorization because they are non-contact and full-field techniques. This is the case of Moiré Interferometry, which is used for many optoelectronic applications as displacement measurements (Wronkowski L., 1995), evaluation of microelectronics devices deformation (Xie H. *et al*., 2004), optical communications (Chen L. *et al*., 2000), strain measurements with Fiber Bragg Grattings, FBGs, (Silva A. F. *et al*., 2011) and spectrography (Kong S. H. *et al*., 2001). In this context, it must be noted that the recent nuclear disaster in Fukushima, Japan, confirms the need of tighter security measures be done within harsh environments (which includes the automobiles) in order to increase both the safety of people and the reliability of vehicles' parts.

## 2. Principles of full-field optical techniques

### 2.1. Holographic interferometry

The holography is a method to store and regenerate all the amplitude and phase information contained in the light which is scattered from an illuminated object. This technology offers the possibility of three dimension photography.

Despite the holography requires coherent light, it was discovered by Gabor in 1948 (Gabor D., 1948), more than a decade before the invention of the laser, which in 1960. By means of holography an original wave field can be reconstructed at a later time at a different location. This technique therefore has many potential applications.

In the year of 1965, when the CW lasers became available, Robert Powell and Karl Stetson published the first work on holographic interferometry (Powel R. L. *et al*., 1965). Using this technique, it is possible record the precise shape and position of a object in two different states, then it is possible compare the two records to measure the movement or deformation, that were displayed as fringes on the image.

In the Figure 1 is shown the optical set-up of holography.

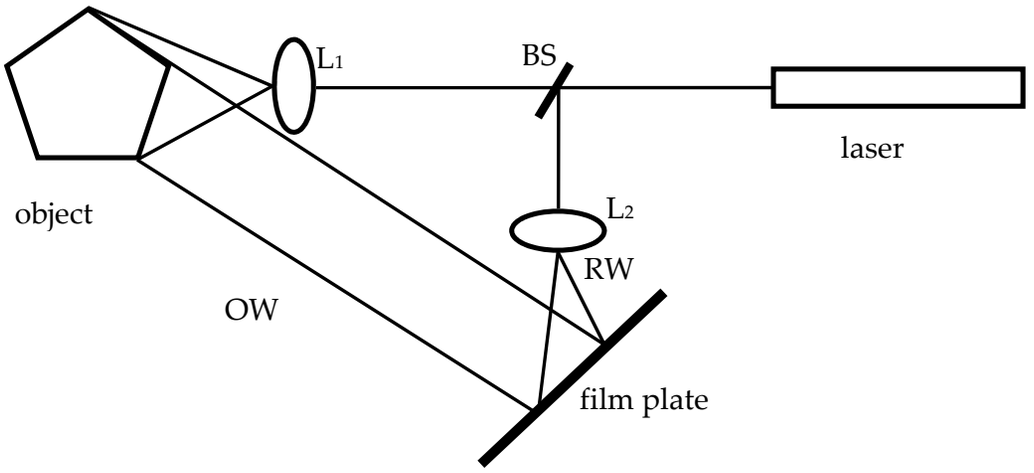


**Figure 1.** Holography configuration to measure the surface displacement.

The laser beam is divided in two beams using a beam splitter (BS). Each of one is opened by two lenses ($L_1$ and $L_2$), on film plate is recorded the interference of two coherent wavefronts: the object (OW) and reference (RW). When the film plate is developed and then illuminated by the reference wavefront, it will be reconstructed a virtual image of the original object. The most used technique for displacement measurement is double exposure or frozen-fringe, which records two holograms on the same film plate, the first one is corresponding to an initial condition of the object and the second one to a displaced or charged condition. The image is reconstructed by a coherent beam illumination; the two reconstructed images will interfere, resulting in a holographic fringe pattern that can be used to measure surface displacements. Each fringe represents a contour of equal displacement of the object, where the value of displacement is one-half the wavelength of the light source used in the recording process (Shang H. *et al*., 2009).

There are others holographic interferometry techniques in which the most relevant are real-time live-fringe and time-average holographic interferometry. The real-time approach requires that the photographic plate must be physically developed in place without changing its position. The single-exposure hologram is made in the regular way and after it is illuminated by the reference beam while the object is illuminate by the original object beam (Cloud G., 1988). The time-average holographic interferometry approach is used for

modal analysis of vibrating bodies. A hologram of the moving body is made with an exposure time lasting over numerous periods of the vibrational motion.

Recent advances in recording materials, lasers and computer allowed more holography techniques being developed, which include: TV holography, digital holography and dynamic holographic interferometry. These techniques open new and challenge fields of research and applications. Nevertheless, this technique has some drawbacks like the displacement components cannot be measured independently in different planes. Another limitation is the strict requirement of vibration (half a wavelength of the illuminating source), if the vibration magnitude is higher occurs decorrelation. As a result, its industrial application as a routine Non Destructive Testing (NDT) technique is restrict, usually these techniques are used in laboratory environment.

## 2.2. Electronic speckle pattern interferometry

Electronic speckle pattern interferometry is a NDT technique which basic concepts were simultaneously developed Mavsky *et al* (Macovsky A. *et al*., 1971) in United States and by Butters and Leendertz (Butters J. *et al*., 1971; Butters N. *et al*., 1975) in England. Later group pursued the development of the ESPI technique, with Lökberg (Lökberg O. *et al*., 1976; Lökberg O., 1985) and Beidermann (Beidermann *et al*., 1975) being important references in this field.

Speckle techniques use the random pattern of dark and bright spots (speckles) that are formed in space when a diffusely reflecting object is illuminated by coherent laser light (laser speckles). A random granular pattern called a speckle pattern is observed when looking, with the eye or with a camera, at a object surface when it is illuminated by a laser - see the Figures 2(a) and (b). The speckles appear only if the surface roughness is greater than the wavelength, $\lambda$, of the light. If the object is imaged, each point P on the detector will gain contribution of light coming from a coherence volume, determined by at least the airy spot and the roughness of the surface (Svanbro A., 2005).

The observed speckle pattern unrepeatable for each illuminated area in the sense that the observed pattern is unique for the microstructure of the specific surface area. Another region will give rise to a totally different random speckle pattern. The speckle pattern is records by a CCD camera and could interfere with a reference wave. If the object suffers a deformation caused by an external load, the speckle pattern will change due the variation of wavefront between the object and reference waves. This deformation could be computed using an operation of digital subtracting between the speckle patterns corresponding to before deformation from the one after deformation. This operation will result in an interferogram, which will be displayed on the monitor as a pattern of dark and bright fringes that are called correlation fringes. ESPI allows displacements in different directions to be measured separately with a high-resolution.

ESPI technique can be sensitive to out-of-plane or in-plane displacement, depending of the used optical set-up. For in-plane displacement measurement (Figure 3), the object lies in the

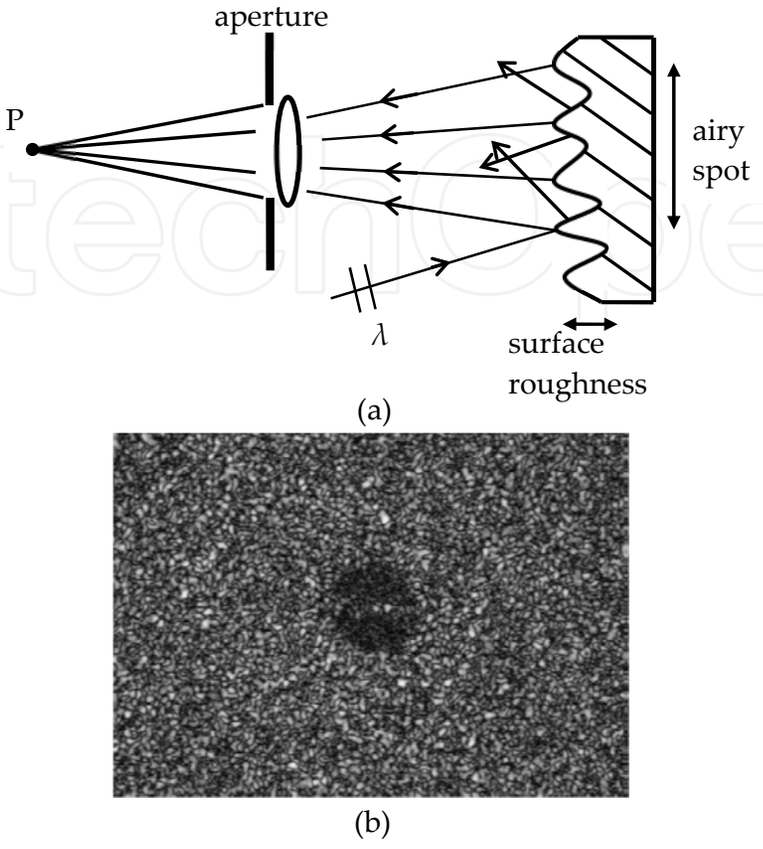


**Figure 2.** (a) The schematic representation of speckle formation and (b) a typical speckle pattern.

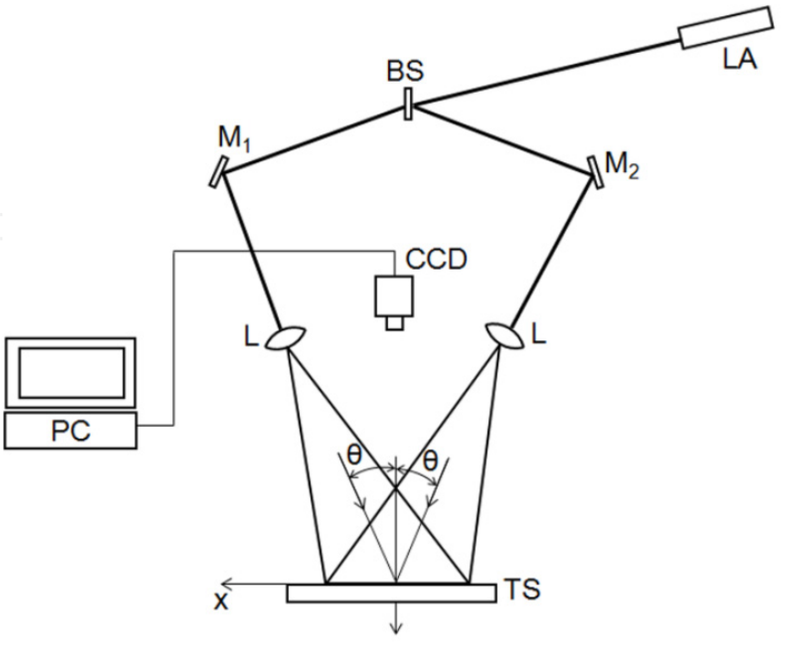


**Figure 3.** A schematic presentation of the optical set-ups used in-plane ESPI (Jones R. *et al*., 1974). LA: laser source, BS: beam splitter, $M_1$ and $M_2$: plane mirrors, L: lens, TS: test specimen or object.

xy-plane and is illuminated by two plane wavefronts, inclined at equal and opposite angles, θ, to the x-axis surface-normal. No separate reference beam is needed at the image plane. The positive y-axis points out of the page, and the center of the viewing lens aperture lies on the z-axis. The phase change $\Delta\phi$ of the wavefront from the object surface before and after deformation can be expressed as:

$$\Delta\phi = \frac{4\pi}{\lambda}\sin(\theta)U \tag{1}$$

where $\lambda$ is the wavelength of the laser, $\theta$ the incident angle, and $U$ is the in-plane displacement component.

For out-of-plane displacement measurement, the object is illuminated by an object which is viewed by a CCD camera (Figure 4). A reference speckle pattern formed by a reference beam is also observed by the camera. So the resultant image is the interference of these two speckle patterns.

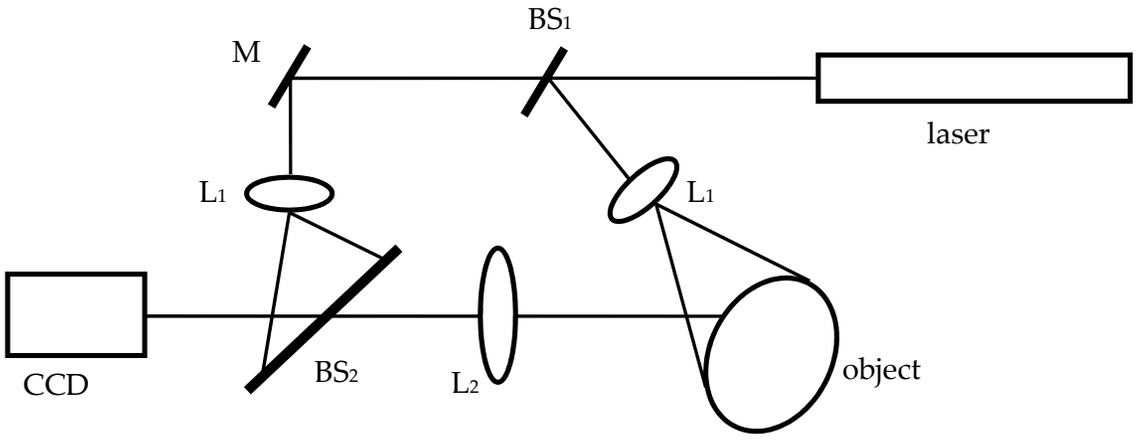


**Figure 4.** ESPI sensitive to out-of-plane displacement. Where $BS_{1,2}$: beam splitter; M: plane mirror; $L_1$: concave lens; $L_2$: convex lens.

The relation between the phase change and the deformation can be expressed as:

$$\Delta\phi = \frac{2\pi}{\lambda}\left[1+\cos(\theta)\right]W \tag{2}$$

where $W$ is the out-of-plane displacement component

## 2.3. Shearography

Shearography technique is particularly interesting because it enables direct measurements of displacement derivatives which are related to the strains (Hung Y. *et al*., 1973; Leendertz, J. A. *et al*., 1973).

The basic principle of shearography, is to carry the rays scattered from one point of the object into interference with those from a adjacent point. To obtained this interference is used a speckle-shearing interferometric camera like the represented in the Figure 5. The optical set-up is similar as that used in common speckle photography, however one half of the camera lens is covered by a thin glass wedge. Thus, the two images focused by each half of the lens are laterally sheared one to other (Gåsvik K. J. *et al*., 2002). The shearing direction is oriented by the wedge position and it is proportional to its angle. If the shearing is in the $x$ direction, the rays from a point $P(x,y)$ on the object will interfere in the image plane with those from a neighboring point $P(x+\delta x,y)$.

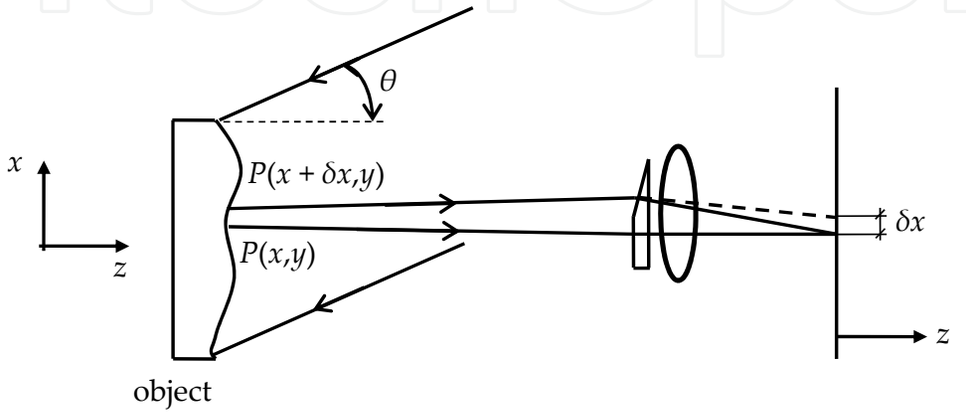


**Figure 5.** The optical set-up of shearography.

When the object is deformed there is a relative displacement between the two points that produces a relative optical phase change $\Delta\phi$ is given by:

$$\Delta\phi = k \times \left\{ \begin{array}{c} \left[1+\cos(\theta)\right] \times \left[w(x+\delta x,y) - w(x,y)\right] + \\ \\ +\sin(\theta)\left[u(x+\delta x,y) - u(x,y)\right] \end{array} \right\} \tag{3}$$

where $\theta$ is the angle of incidence and $u$ and $w$ are the displacement components in the $x$-and $z$-directions, respectively. If the shear $\delta x$ is very small, the relative displacements may be approximated by the displacement derivatives and thus Equation (3) becomes:

$$\Delta\phi = k\{\left[1+\cos(\theta)\right]\frac{\partial w}{\partial x} + \sin(\theta)\frac{\partial u}{\partial x}\}\delta x \tag{4}$$

By rotating the camera 90º around the $z$-axis, $u$ in Equation (4) is replaced by $v$, the displacement component in the $y$-direction.

## 2.4. Moiré methods

The word Moiré derives from the French term meaning wet silk or fringe patterns produced by the interference of aligned fibers in thin tissues. In Engineering, Moiré refers to a technique for experimental analysis for determining the displacement or deformation from a

set of interference fringes resulting from the superposition of two systems - one in the deformed specimen and the other that is undeformed can be used as reference. Moiré techniques have appeared in the field of optics since nineteenth century (Rayleigh L., 1874). The Moiré techniques allow the measurement of deformations which occur when an object is subjected to applied charges. These methods can measure out-of-plane and in-plane displacements. The displacements are measured simultaneously over the whole view field and the measurement data are exposed as contour maps of displacements. One of most important Moiré method is the Moiré interferometry that was performed by Post (Post D. *et al*., 1994) in 1980 and represents one the most important advances in optical techniques applied to experimental stress analysis in the last decades. The Moiré interferometry principle is based in the interference of two coherent light beams or lasers beams. This interference produces regions in space of constructive and destructive interference where two equal coherent beams intersect. The most important advantages of Moiré interferometry compared with other optical methods are: excellent fringe contrast, high sensitivity and special resolution (typically 0.417 μm per fringe), dynamic range of measurement and high signal-to-noise ratio (Ribeiro J. E., 2006). On the other hand, an important disadvantage of this technique is the need of a high-frequency grating replication onto the sample surface before the measurement begins. The replication of grating could restrict its application in cases where the replicated grating may considerably change the stiffness of the testing sample, another difficulty of this process is the need of a technician with experience implement the replication and it is very laborious.

To measure in-plane displacement with Moiré interferometry are used two symmetrical incident beams of mutually coherent light (Post D. *et al*., 1994), see the Figure 6.

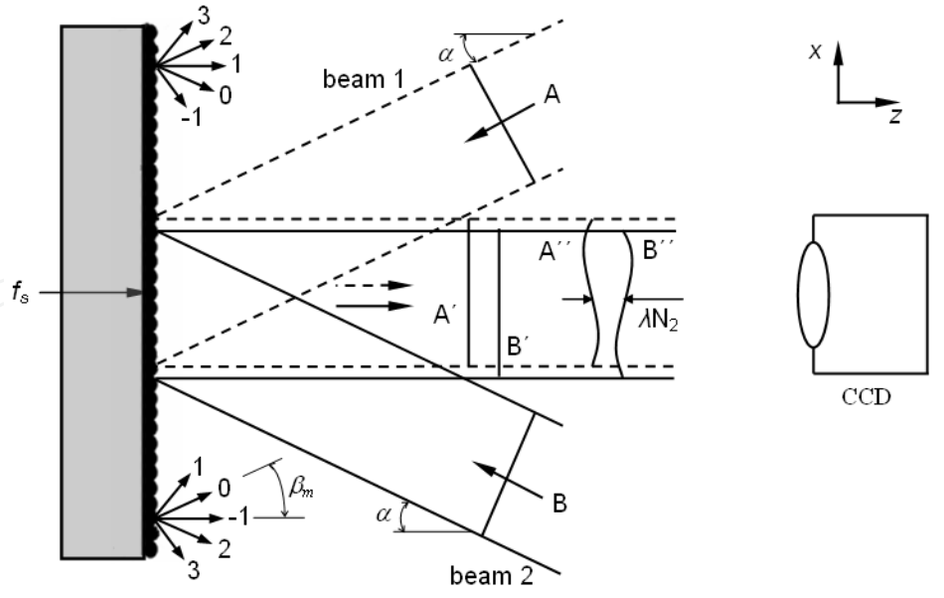


**Figure 6.** Schematic representation of Moiré interferometry principle (Post D. *et al*., 1994).

The diffraction equation for the represented grating is:

$$\sin(\beta_m) = \sin(\alpha) + m\lambda f_s \tag{5}$$

where $\beta_m$ are angles of diffracted beams, $\alpha$ is the angle of incident beam, $m^{th}$ the diffraction order, $\lambda$ the laser wavelength and $f_s$ is the grating frequency of specimen.

When the equation (5) is satisfied, the ±1 order diffraction beams will emerge normal to the specimen grating, producing a uniform intensity throughout the field (null field) (Shang H. *et al.*, 2009).

The obtained displacement fields allow the calculation of components orthogonal direction ($x$, $y$) and they can be expressed as:

$$\begin{aligned} u &= \frac{1}{f} N_x = \frac{1}{2f_s} N_x \\ v &= \frac{1}{f} N_y = \frac{1}{2f_s} N_y \end{aligned} \tag{6}$$

By differentiation of displacements is obtained the corresponding strain components:

$$\begin{aligned} \varepsilon_x &= \frac{\partial u}{\partial x} = \frac{1}{2f_s} \frac{\partial N_x}{\partial x} \approx \frac{1}{2f_s} \frac{\Delta N_x}{\Delta x} \\ \varepsilon_y &= \frac{\partial u}{\partial y} = \frac{1}{2f_s} \frac{\partial N_y}{\partial y} \approx \frac{1}{2f_s} \frac{\Delta N_y}{\Delta y} \\ \varepsilon_{xy} &= \frac{1}{2}\left( \frac{\partial u}{\partial y} + \frac{\partial v}{\partial x} \right) \approx \frac{1}{2f_s}\left( \frac{\Delta N_x}{\Delta y} + \frac{\Delta N_y}{\Delta x} \right) \end{aligned} \tag{7}$$

where $N_x$ and $N_y$ are fringe orders in $x$ and $y$ direction, respectively.

To measure out-of-plane deformation and obtained the shape of a body is frequently used the well-kwon experimental technique Shadow Moiré (Takasaki H., 1970). The optical set-up is schematically represented in the Figure 7.

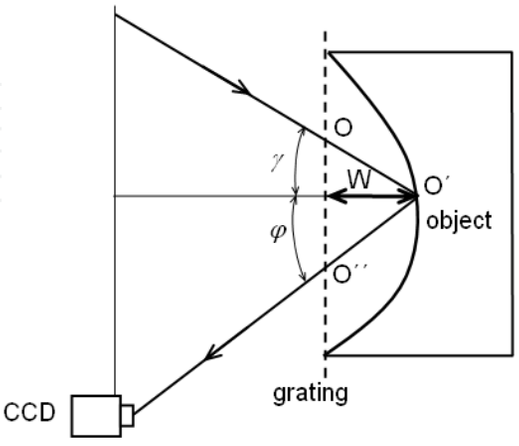


**Figure 7.** An optical set-up of Shadow Moiré.

The grating lying over the curved surface is illuminated under the angle of incidence $\gamma$ (measured from the grating normal) and viewed under an angle $\varphi$ (Gåsvik K. J., 2002). From

the Figure 7, it possible to observe that a point O on the grating is projected to a point O′ on the surface which by viewing is projected to the point O′′ on the grating. This is equivalent to a displacement of the grating relative to its shadow equal to:

$$W = \frac{np}{\tan(\gamma) + \tan(\varphi)} \tag{8}$$

where $W$ is the out-of-plane displacement, $n$ is the order of fringe and $p$ is the pitch of the grating.

## 2.5. Digital Image Correlation (DIC)

Digital image correlation belongs to the class of non-contacting measurement methods that were developed by Sutton (Sutton M. A. *et al*., 1983; Sutton M. A. *et al*., 1986; Sutton M. A. *et al*., 1991; Sutton M. A. *et al*., 1988) and by Bruck (Bruck A. *et al*., 1989), in which acquires images of an object, store these images in digital form and perform image analysis to obtain full-field shape, deformation and motion measurements (Sutton M. A. *et al*., 2009). In this method is used a mathematical correlation to estimate the displacement in the plane surfaces or structures of components subject to mechanical or thermal stresses. This technique is based in the use of random patterns on the surface of the components or structures. The technique compares two images acquired at different states, one before deformation (reference image) and other after deformation (deformed image) (Hu T. *et al*., 1985).

In this technique the object is illuminated by an incoherent light source and the patterns of intensity results from the surface texture. These patterns of intensity, which would have a random distribution, are subdivided into smaller areas. Each subregion [originally defined in the image recorded] is then compared with images obtained by correlation between two different states of deformation in the object. If $f(x,y)$ is a discrete function that defines the grayscale of pixel on the original image and $f^*(x^*,y^*)$ is the grayscale of pixel on the final image (Marcellierl H. *et al*., 2001). The relation between the two functions is defined by:

$$f^*(x^*, y^*) = f[x + u(x,y), y + v(x,y)] \tag{9}$$

where $u$ and $v$ represent the displacement field.

The determination of the displacement field is obtained by correlation between the random pattern of the initial image (reference) and its transform (deformed). This operation is performed for all patterns that meet in the center of the virtual grating on the initial image so as to obtain all the displacement field of each grating element.

Considering the displacement field for a random pattern, that is uniform and bilinear along the axes $x$ and $y$, and given by:

$$u(x,y) = a_u x + b_u y + c_u xy + d_u \tag{10}$$

$$v(x,y) = a_v x + b_v y + c_v xy + d_v \tag{11}$$

The correlation between images of before and after deformation can be expressed as:

$$C = \frac{\sum_{x,y\in S}[f(x,y)f^*(x^*,y^*)]}{\left[\sum_{x,y\in S} f^2(x,y)\sum_{x,y\in S} f^{*2}(x^*,y^*)\right]^{\frac{1}{2}}} \tag{12}$$

where $f(x,y)$ and $f^*(x^*,y^*)$ are intensity distributions of speckle images before and after deformation, respectively. When $C$=1, the two images have the best correlation, i.e., they become identical.

This method has many advantages compared with others, which is possible to detach the follow: the cost of DIC is relatively low when compared to moiré and ESPI, because optical set-up is simple and it is not necessary a coherent light source; the resolution of DIC depends not only on the optical magnification, but also on the image processing (sub-pixel algorithms). Using a zoom lens and high resolution imaging system including CCD, can be reached a resolution of sub-micron.

## 2.6. Phase measurement techniques

In last decades, have been developed different techniques for quantitative phase measurement from fringe patterns (Robinson D. W. *et al*., 1993; Creath K. *et al*., 1994). These techniques are classified in two groups: spatial and temporal. In the spatial phase-measurement techniques, the phase information is extracted from a single interferogram which has a large number of tilt fringes that are used as a carrier frequency. For the temporal phase-measurement techniques, the phase is measured using a single point in an interferogram as the phase difference between the analyzed and reference beams is changed in a controlled way by the means of a piezoelectric device. The N-frame techniques measure a sequence of interferograms with known phase shifts techniques and they are the most popular type of these (Creath K. *et al*., 1996).

The phase shifts or phase-shifting are the techniques extensively used in automatic fringe analysis of interferogram. It has considerably improved the accuracy of optical techniques, allowing the fast visualization of results. In the phase-shifting technique, the phase change is introduced usually by a calibrated phase steps. The phase of the whole image can be computed by analyzing the intensity patterns taken at different step.

The intensity or irradiance recorded by a detector for a single interferogram can be written as:

$$I(x,y) = I_0(x,y)\{1 + \gamma(x,y)\cos[\varphi(x,y) + \alpha_i]\} \tag{13}$$

where $I_0(x,y)$ is background contribution, $\gamma(x,y)$ is the interference fringe amplitude, and $\phi(x,y)$ is the function of fringe phase, $\alpha_i$ the amount of phase shifting, $(x,y)$ the coordinates of the image plane.

The most common phase-shifting technique is the four-point which uses four intensity values with $\pi/2$ relative phase shifts between steps. It is written in the form:

$$\varphi = \text{atan}\left(\frac{I_4 - I_2}{I_1 - I_3}\right) \tag{14}$$

where $I_1$, $I_2$, $I_3$ and $I_4$ are intensities recorded in the detector for four different interferograms with phase shifts of $\alpha$=0, $\pi/2$, $\pi$ and $3\pi/2$.

Analyzing the equation (15) it is possible to verify that there are discontinuities for the phase values of $\pi$ and $-\pi$ which results from the atan function. These discontinuities are eliminated by using algorithms developed for this purpose (unwrapping). Thus, the absolute phase maps can be computed by phase unwrapping to reveal the accurate displacement field.

## 3. Industrial applications of full-field optical techniques

### 3.1. Vehicle shape measurement

In the automotive industry, it is essential measuring with accuracy the 3-D shapes of objects to ensure product development and manufacturing quality.

Traditionally, the most used technique to measure the vehicle shape is the use of structured method combined with photogrammetry. In this case are used some targets that are fixed on the vehicle body which allow the coordinate transformation from local to global. A structured light is projected on the vehicle surface combined with absolute phase measurement and phase shifting using fringe frequency change to determine the local coordinate pixel by pixel at one view direction (Chen F. *et al*., 2000). The process is repeated for more than a two hundred views to cover hall vehicle. After these measurements are obtained a cloud of points that are patched together using a least mean squares method.

Recently, have been developed new progresses in 3D shape measurement (Zhang S., 2010), in this process is used a projector to project sinusoidal patterns and is called digital fringe projection technique, if is adopted a phase-shifting algorithm to, this technique is called digital fringe projection and phase-shifting technique.

In the digital fringe projection technique, a computer creates the digital fringe patterns which are composed of vertical straight stripes that are sent to a digital video projector. The fringe images (vertical straight stripes) are projected onto the object, which are distorts by the surface profile, then a CCD camera captures the distorted fringe images for the computer that analyzes the fringe images to obtain 3D shape information based on the deformation using triangulation. In this process is frequently used phase shifting algorithms which improve the optical metrology resolution (Huang P. S. *et al*., 2006).

### 3.2. Measurement of residual stresses

The residual stresses can be defined as those which remain in the material or component after the manufacturing process and in the absence of external forces and thermal gradients

(James M. R. *et al*., 1996). The manufacturing processes are the most common cause of residual stresses and some examples of manufacturing processes that can introduce residual stresses in the produced components are casting, welding and machining, all of them are used in automotive industry. However, the residual stresses can also arise for maintenance or repair operations. Sometimes, these stresses can also be induced in service during installation or by occasional overloads.

The effects of residual stresses can be beneficial or detrimental, depending on its magnitude, sign, and its distribution. In most cases residual stresses are harmful because they overlap with the operating stresses. However, they could be also beneficial, especially by allowing the increased of the fatigue limit in components which are dynamically requested. Another particularly important feature concerning the residual stress is that its presence usually is undetected until the malfunction or failure occurring.

There are currently different techniques for measuring residual stress, such as the contour method (Richter-Trummer V. *et al*., 2011), the hole-drilling with strain gages or optical processes which use visible radiation of light (Ribeiro J. E., 2006), X-ray and neutrons diffraction, magnetic techniques and ultra sounds (James M. R. *et al*., 1996). Some of them use mechanical processes to stress release in order to measure the residual stresses while in others it detects its presence by the effect of material properties. However, none of which is universally applicable, despite the most used technique to measure residual stresses is the hole-drilling method.

The hole-drilling method is an experimental technique used for measuring the strains on surface caused by the stress release. These strains can be measured using electrical discrete transducers or calculated from the displacement field on surface. The optical techniques used for measuring the displacement have great advantages compared with other techniques, emphasizing the performing of a global or field measurement and without contact. These techniques allow in-plane and out-of-plane measurements with a resolution that can be variable, ranging from a low resolution (tenths of mm) until very high with a magnitude of used light wavelength (a few tenths of a micrometer). The most used optical techniques combined with hole-drilling method (Ribeiro J. *et al*., 2009) are the Moiré interferometry (Ribeiro J. *et al*., 2009) and the ESPI (Cheng P. *et al*., 2008) to measure residual stresses.

In this chapter a process to measure residual stresses with optical techniques (in-plane ESPI and Moiré Interferometry) is developed and combined with the hole-drilling method. Measurements were carried out on a ring and plug specimen, constructed to produce well known residual stress fields. The calibration coefficients were obtained by numerical simulation with a Finite Element Method (FEM) code. For these measurements were prepared two optical set-ups, one for Moiré Interferometry (Post D. *et al*., 1994), see in the Figure 8, and the other for double-illumination ESPI (Jones R. *et al*., 1974), see in the Figure 3. Both were used to measure the in-plane displacements generated by residual stress release. Image processing algorithms, involving filtering, phase calculation and unwrapping, and spatial differentiation were used in data post-processing to transform surface displacement into residual stress fields.

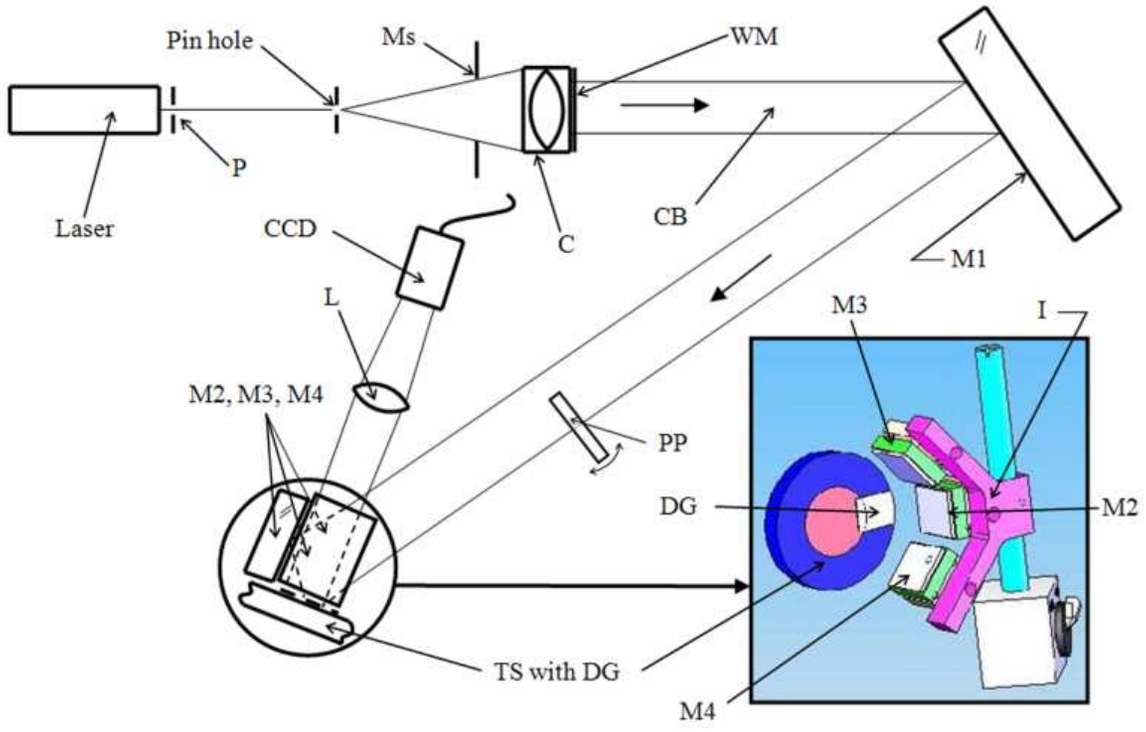


**Figure 8.** The schematic presentation of the moiré interferometry optical set-up used (Ribeiro J. *et al.*, 2011).

Where LA is the laser source, Ms is a mask, C is the collimator, WM is a window mask, CB is the collimated beam, M1, M2, M3 and M4 are plane mirrors, PP is a parallel plate glass, L is a lens, TS is the test specimen, DG is the diffraction grating, and I is the interferometer.

The stresses were released according to the conventional procedure used with strain gages. Drilling a hole on the surface of a specimen with residual stresses produces a stress relaxation around it. The corresponding deformation was assessed in this work with an optical technique. In the Figure 9 is possible to observe the system used to measure the residual stresses in the ring and plug specimen using the Moiré Interferometry an ESPI.

In the ESPI measurement an initial specklegram is acquired and saved. Then, the drill is placed in front of the test specimen and a small hole is drilled to a given depth. Next, the drill is removed and another specklegram is acquired. The interferogram resulting from the correlation of the two recordings leads to the surface displacements caused by the stress relaxation. In this case the surface information is codified in the speckle patterns.

For the Moiré Interferometry a high frequency grating was previously bonded on the surface of the specimen. The grating used was a 1200 lines/mm, obtained by aluminum vaporization on the top of an epoxy replication of a master grating. The set-up proposed by Post (Post D. *et al.*, 1994) was used in the virtual grating generation by laser interferometry. The first recording was obtained by superposition of the virtual grating over the object replication grating. Then, a hole is drilled at the desired place, and the Moiré fringes due to stress relaxation are obtained and recorded. A tiltable parallel plate glass was used to promote phase modulation with a four image phase calculation algorithm (Creath K. *et al.*, 1996).

In both cases, the residual stress field was computed establishing an appropriate stress–displacement relationship by a FEM code.

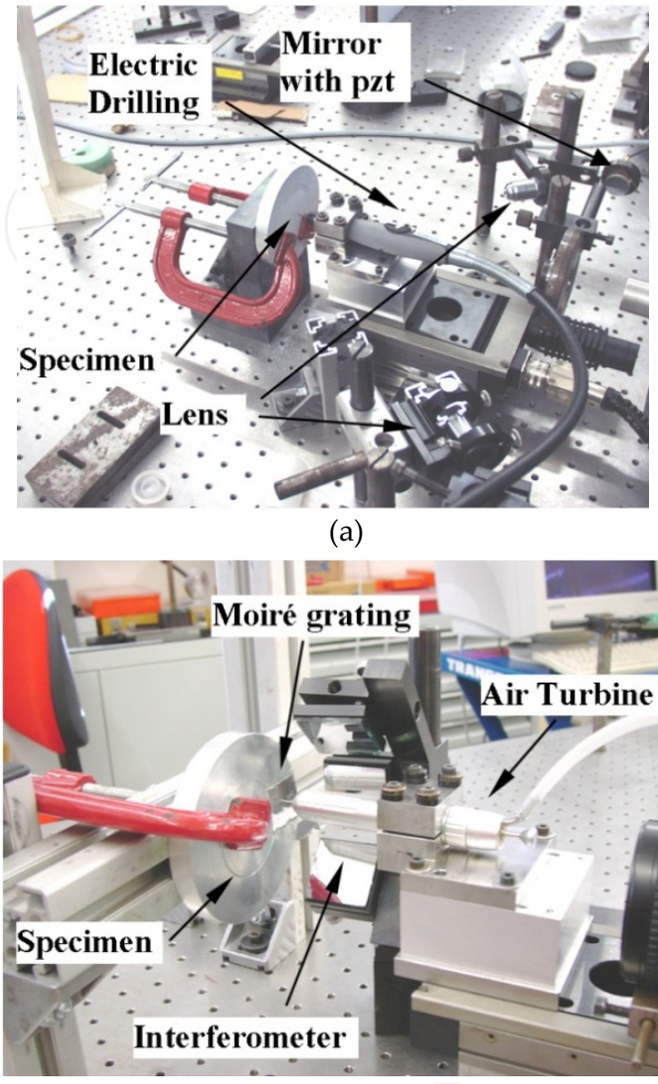


**Figure 9.** An apparatus to measure residual stresses using the hole-drilling technique associated to: (a) in-plane ESPI; (b) Moiré Interferometry (Ribeiro J. *et al*., 2011).

The ring and plug specimen has a closed form solution (Lamé M. G., 1852) for the residual stresses, and relatively simple stress distribution. In the plug the stress is constant, in the ring only depends on the radial position. The specimen was prepared in agree of the reference (Ribeiro J. *et al*., 2009). After the specimen preparation and its stress state control, several measurements of residual stresses were made using optical techniques and the hole-drilling method. The optical set up used to measure residual stresses with in-plane ESPI and Moiré Interferometry are schematically represented in the Figures 6 and 8, respectively. The Figure 9 shows details of both set-ups with the additional system for drilling of holes.

To calculate the displacement field eight images should be recorded in both techniques, at different phase shift, being half of them before and the remaining after hole drilling. In ESPI

the displacement field is calculated by subtracting the speckle phase maps obtained before and after strain relaxation.

The Figure 10 summarizes the results obtained for residual stresses measurements. In this graphic presentation the solid lines represent the stresses calculated by the close form solutions given by Lamé (Lamé M. G., 1852). The experimental data is represented by dots. In all the cases the error was less than 17%, with most of the measurements being around 5% of error.

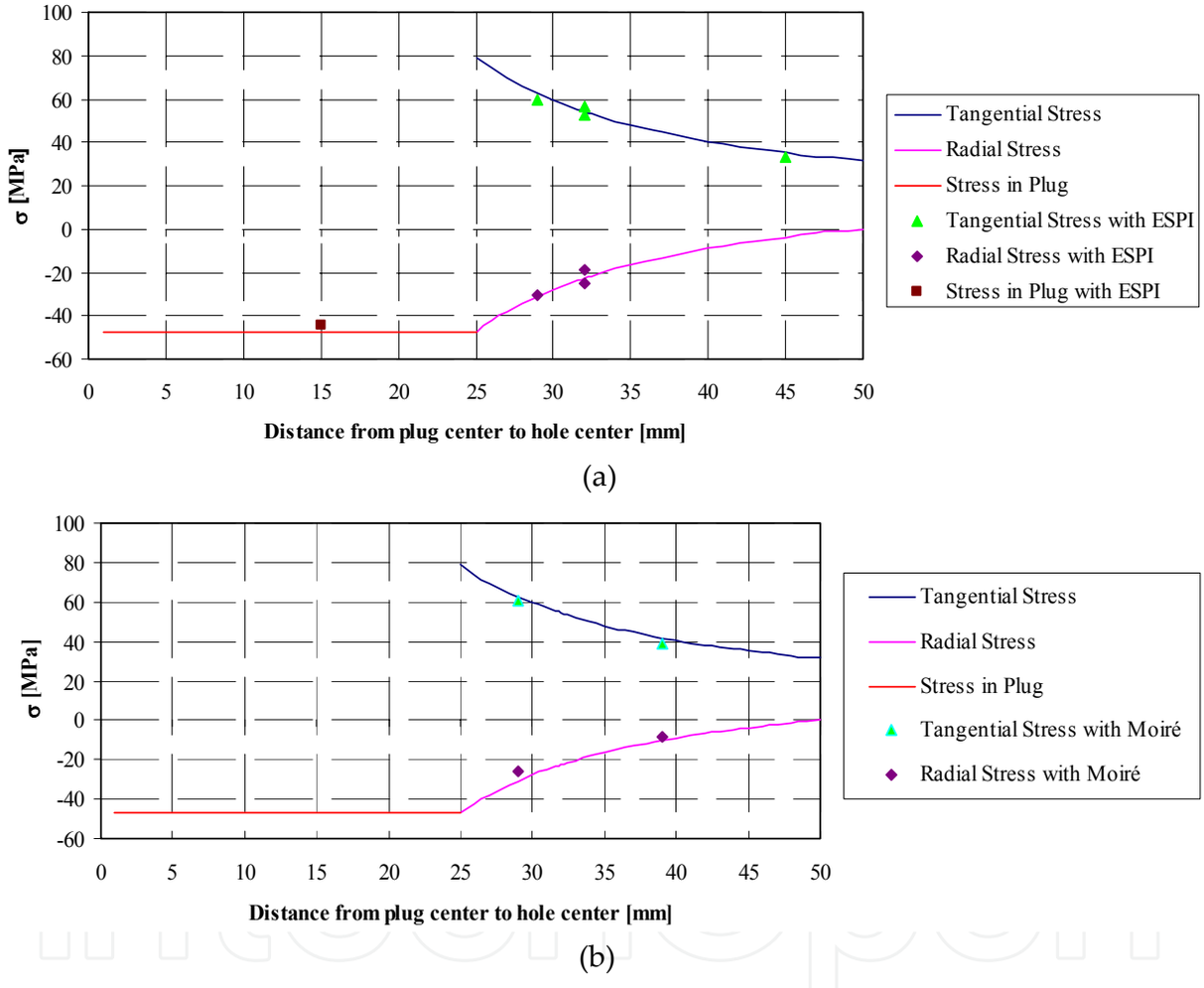


**Figure 10.** A closed form solution and experimental measurements with (a) ESPI and (b) Moiré.

In this work an experimental methodology for residual stress assessment is presented using optical techniques with the hole drilling method. These methods were tested with a well known residual stress field in a ring and plug specimen. The experimental results obtained with in-plane ESPI and Moiré Interferometry are in good agreement with the closed form solution. These optical techniques are a very interesting alternative to the traditional hole-drilling method with strain gages, and present some advantages, it is a global measurement, has better resolution and allows measurements closer to the hole edge.

# 4. Other optical techniques for the automotive industry

## 4.1. Smart materials based on FBGs

There are available a wide variety of optical fiber sensors, which can be divided in three categories. The first category includes the external type (also known as extrinsic) where the fiber is only used to transfer the measured information from a distant location (Beard P. C. *et al*., 1996). The intrinsic category includes the optical fibers where at least one optical property (with the consequence of modulating the light) is affected in result of the measured information (Boerkamp M. *et al*., 2007). Finally, it exists the hybrid category that includes all the situations where the light is transferred for further optoelectronic conversion on a distant receiver (Yau S.-K. *et al*., 1983). In this context, the Fiber Bragg Gratings (FBGs) are the most suitable sensing elements with an increased usage for structural measurements due to their high performance in terms of the sensitivity and linear response. These sensors differ from conventional optical fiber sensors approaches because their optical signal is not based on power amplitude but instead on spectral changes. This factor is important for embodiment techniques into structures (for example, in the vehicles' structures) since the bends on the optical fiber introduce intensity changes (Kung P., 2009). Moreover, the FBGs are suitable sensing elements for doing physical measurements where a kind of displacement is available. Examples of such applications found in the literature include the measurements of strain (Ling H. Y. *et al*., 2006), pressure (Peng B. J. *et al*., 2005), force (Zhao Y. *et al*., 2005), acceleration (Antunes P. *et al*., 2011), tilt rotation by an angle (Xie F. *et al*., 2009), temperature (Gu X. *et al*., 2006) humidity (Arregui F. J. *et al*., 2002), magnetic fields (Orr P. *et al*., 2010), cardiorespiratory function (Silva A. F. *et al*., 2011), gait function analysis (Rocha R. P. *et al*., 2011) and integration on wearable garments (Carmo J. P. *et al*., 2012b).

Looking to the technology point of view, the FBGs consists on periodic changes of the refraction index allong the fiber core. These changes are "shaped" by exposing the fiber to intense ultra violet (UV) light with a suitable interferometer mask (Hill K. O. *et al*., 1997). The typical lengths of produced gratings are in the range of few millimetres and are characterized by a narrowband resonance spectral reflection. The resonance behaviour depends on grating pitch and on their axial variation because the resonance behaviour strictly follows external actions in the exact proportion as the silica matrix surrounding the gratings (Kersey A. D. *et al*., 1997). The ultimate effect of the resonances is the reflection by successive and coherent scatterings from the index modulation of a narrow band of the incident optical field injected into the fiber (Hill K. O. *et al*., 1997). In a FBG, the strongest interaction or mode coupling responsible for the reflected light occurs at a well-known wavelength, $\lambda_B$ [nm], also known as Bragg wavelength. The Bragg's spectral component depends directly from the grating period of the FBG, $\Lambda$ [nm], from the modal index, $n_{eff}$, also known as effective refractive index of the FBG, and is given by:

$$\lambda_B = 2 n_{eff} \Lambda \tag{15}$$

The shift in the wavelength, $\Delta\lambda_B$ [nm], with respect to the cross sensitivity with the temperature and the axial strain changes, $\Delta T$ [K] and $\Delta\varepsilon$, (respectively) is given by (Wei C. L. *et al*., 2010; Silva *et al*., 2010):

$$\frac{\Delta\lambda_B}{\lambda_B} = (1-\rho_\varepsilon)\Delta\varepsilon + (\alpha+\xi)\Delta T \tag{16}$$

where $\rho_\varepsilon$ is the photo-elastic coefficient of the fiber, $\alpha$ is the thermal expansion coefficient of the fiber material, and $\xi$ is the thermo-optic coefficient of the fiber material. Typical value for a 1550 nm FBG fabricated in a silica fiber, the temperature and the axial strain sensitivities are respectively $\Delta T \approx 13$ pm.ºC$^{-1}$ and $\Delta\varepsilon \approx 1$ pm.με$^{-1}$ (Silva A. F. *et al*., 2011). It mandatory to compensate the temperature offset when the measurements consist only on strains. The Figure 11 illustrates a FBG structure after being written on an optical fiber. This figure also illustrates that the injection of a broadband pulse on the FBG results in a reflected beam located around the Bragg wavelength, $\lambda_B$ . It is then possible to determine the exact strain by measuring the reflected spectra and/or the shifting produced in the Bragg wavelength (Zhou W. *et al*., 2010).

It must also be noted that the absence of mechanical steps on sensor's fabrication results in the possibility to fabricate high sensitivity sensors with high reproducibility of their characteristics (Hill K. O. *et al*., 1997). However, the most important features that made FBG based systems a wide established technology were their electrically passive operation, electromagnetic interference immunity, compact size, self referencing capability, and more important, inherent multiplexing-ability, which enables a wide number of sensors in a single fiber as well as Bragg a single interrogation system (Wang Q. *et al*., 2007).

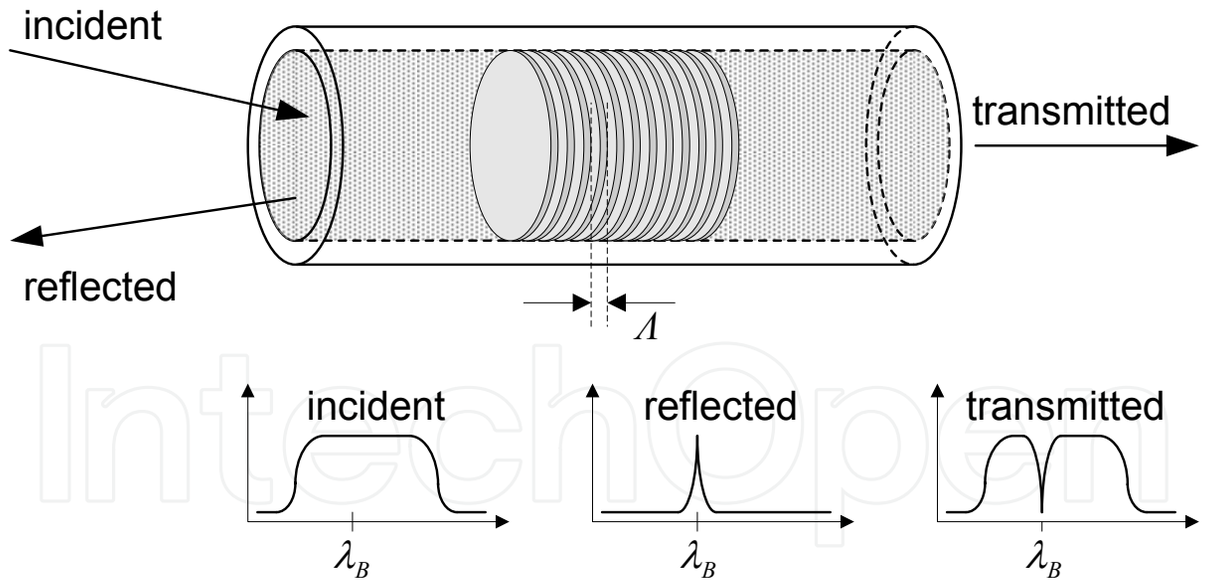


**Figure 11.** Illustration of working principle of FBGs.

The artwork illustrated in the Figure 12(a) helps to understand how to apply FBGs on vehicles. The use of a polymeric carrier with elastic properties, such as those developed and fabricated by Silva (Silva A. F. *et al*., 2012) in polychloroethanediyl (polyvinyl chloride, or simply PVC) (Saeki Y. *et al*., 2002) with one or more embedded FBGs can be used to sense deformations along the vehicle structure. The beauty of all is in the intrinsic simplicity, e.g., the whole system require only the use of a broadband optical source (and centred at the 1550 nm),

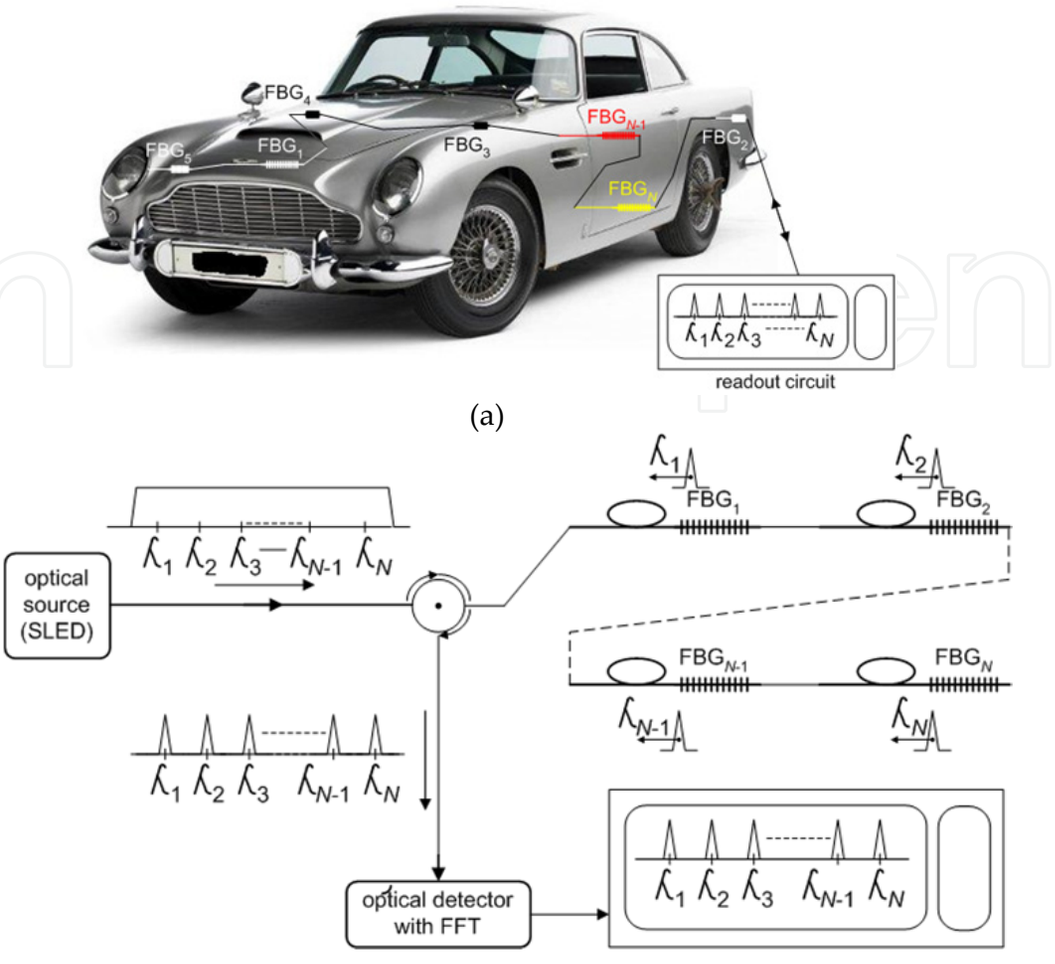


**Figure 12.** (a) Application of FBGs for monitoring structural deformations on vehicles, (b) Optoelectronic monitoring system based on FBGs for online/offline monitoring of vehicles.

a single optical circulator, few FBGs centred at different Bragg wavelengths $\lambda_B$ and a optical receiver with enough spectral resolution $R$ (Carmo J. P. *et al.*, 2012a) spanned along the wavelength range to cover all Bragg wavelengths. The Figure 12(b) illustrates an example for both online (i.e., during the motion of the vehicles) and offline (i.e., with the vehicle parked for maintenance by a mechanic) monitoring. In terms of technology and systems there are available a wide number of companies that offer optical sources, FBGs, optical circulators and optical sources at reasonable costs. Of course, the most challenging task is embedding FBGs into the flexible carriers. However, this problem was already addressed and the complete details can be found on (Silva A. F. *et al.*, 2012). The optical source Superluminiscent LEDs from DenseLight Semiconductors manufacturer can constitute a possibility due to its capability to generate broadband light beams with wavelengths in the range 1530-1570 nm with a maximal power of 8 mW (Denselight, 2012). Additionally, this optical source also presents a full width at half maximum (FWHM) of 60 nm with a maximum ripple of 0.2 dB. The FBGs can be acquired with the FiberSensing company (FiberSensing, 2012), which offers to their clients the possibility to write gratings in

hydrogen loaded standard telecommunication fiber (Corning SMF28e+) using the phase mask technique and a pulsed Excimer Laser. The I-MON 80D interrogation monitor from Ibsen Photonics (Ibsen, 2012) is an interesting option to implement the optical receiver because it is especially suitable for real-time spectrum monitoring of signals acquired from FBG sensors. One of the characteristics of this optical detector is operating in the wavelength range of 1529-1561 nm with a resolution of 1 pm for at least 20 dBm of optical power. Moreover, the maximum wavelength drift of this optical detector is around 2 pm per ºC with a dynamic range of 30 dB, an input optical power in the range 10-50 dBm and a power consumption of 250 mW. Finally, the optical circulators can be found in the manufacturer ThorLabs with interesting costs and low losses (ThorLabs, 2012). The 6015-3 optical circulator constitues an interesting option because it operates in a relatively broadband wavelength range with isolation higher than 40 dB (e.g., between 1525 nm and 1610 nm according the manufacturer). Simultaneously, the loss due to the polarization sensitivity of this component is very low (e.g., less than 0.1 dB). Moreover, the delay spread is also very low (e.g., less than 0.05 ps). To finish, this optical circulator provides a high return loss (e.g., higher than 50 dB) for optical powers up to 500 mW .

## 4.2. Spectroscopy

Spectroscopy is the science investigating the interaction between radiation and matter centered on the wavelengths. The propagation of energy occurs through waves that can be classified either as a function of the frequency υ, or the wavelength $\lambda$. The relation between these two properties is given by the following equation: $c=\lambda v$ where $c$ is the speed of light ($\approx 3\times10^{8}$ m.s$^{-1}$). Radiation, within the context presented in this paper, describes how photons propagate through a medium and is given by $E=h.v$ where $E$ is the energy associated with the photons emission and h is the Planck constant and is equal to $6.626/10^{34}$ J.s. With these equations it is possible to correlate the different properties, which are the foundations of the spectrography laws. The all-generic purpose spectroscopic techniques used more often are the X-ray diffraction (XRD, from $10^{-3}$ to 10 nm), ultraviolet (UV, from 10 to 400 nm), visible (VIS, from 380 to 780 nm) and infrared (IR, from 0.7 to 1000 μm).

Paint is essentially made of three components: binders, pigments (responsible for the color) and solvents. From these components of paint, attention will only be given to the one that define colors by selectively absorbing the visible wavelengths. Pigments are mainly composed by groups of aromatic rings linked by chromophores (may be azo compounds, carbonyl groups, basic, etc.). The mechanism responsible for providing a color to a pigment is the combination of two molecular components: the chromophores and the auxochromes (Zhang Y. *et al*., 1995). Chromophores are the part of the molecule that gives the necessary conjunction to obtain colors. The auxochromes are a group of atoms linked to the chromophores that complement the action of the latter by performing the necessary changes, within the system's total energy, resulting in the final color. An example in basic dye (where chromophores have thiazine group), is seen in the Figure 13 (Lachheb H. *et al*., 2002).

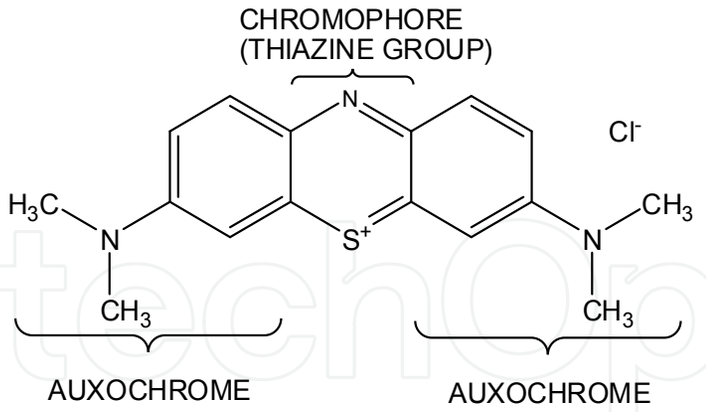


**Figure 13.** Example of the presence of chromophores and auxochromes in basic blue 9.

From the mentioned spectroscopic techniques, only the UV/Vis and IR, allow the detection of colors from a specific chemical compound by analyzing the intensity level of the absorption band. Therefore, when a chemical compound absorbs within a specific spectrum, it means that it will have the complementary color. As an example, if the most intense absorption band in a UV/Vis spectrum is in the 600 nm, i.e. absorbs the orange color, this means that its color will be the orange's complementary; which is blue. Consequently, when these analyses are done, it is not the color that it is determined directly but, instead, the chemical composition of the compound.

The main performance parameter is the spectral resolution $R=\lambda/\Delta\lambda$, where $\lambda$ [m] is a particular wavelength setting, and $\Delta\lambda$ is the smallest discernible wavelength difference for the given $\lambda$. High-performance spectrometers can reach very high resolutions, greater than $R=10^6$ (Lindblom P. *et al*., 1990) but are macrosized and expensive. However many times, mainly in the industry due to its intrinsic fast-moving nature, it is not required such a high level of resolution. Microspectrometers on the other hand, because of their small size limitation, have resolutions which are more suitable for rapid color evaluation without the excessively high-quality optical performance for such industrial applications. Spectrometers built using integrated silicon microsystems, have a spectral resolution $R<50$ and for MEMS based systems, $R=100$ (Carmo J. P. *et al*., 2012a). Color identification is a process being widely used in many different fields. A very interesting and challenging one is to apply microspectrometers in industrial environments. Some industries are more suitable for such color evaluation and measurement procedures such as the: paint, biomedical, textile, ceramic, glass, chemical, etc. Industrial production processes permit the possibility to measure different chemical compounds by spectroscopic methods, which allow studying the colors and according to the needs, different wavelengths spectrum are used. In this context, the color identification and evaluation in the different states of matter is a process with increasing focus by the industry. Within the chemical industry, where is included the textile, polymeric and the ceramics industries, as well as the biomedical, are some of the ones that need more of these kind of characterizations. In the mentioned industries, there is a flagrant need to analyze and detect the presence of different chemical compounds in laboratorial

environment, by spectroscopy techniques that allow the study of the different colors. These different spectral analysis techniques demand very expensive, bulky equipments, hardware and software (Wolffenbuttel). A tunable microspectrometer for non-extremely demanding optical resolutions industrial applications is a very interesting solution, especially for end-use customer services offered by the paint industry (Xie F. *et al*., 2009). Customization of colors can be done quicker, and cheaper, by analyzing on an early stage, the development of any color is having. This procedure can potentially save money and time, which is of extreme value in the industry. Any necessary correction can be performed at any stage of color design. An application in the automotive industry can be seen in Figure 14.

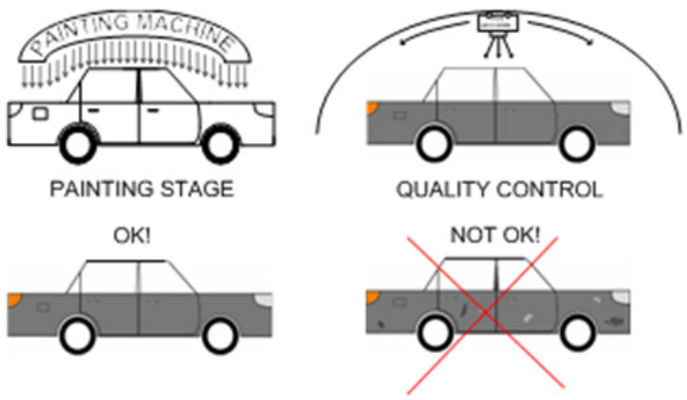


**Figure 14.** Microspectrometer use in color evaluation in the automotive industry.

The Figure 14 illustrates from the top to bottom and left to right, a practical use for microspectrometers in the automotive industry. First, the cars are painted by an industry standard process and then, the color of the car is evaluated throughout its entire painted areas, by a microspectrometer in scanning-type movements, in real-time. If the automatic color evaluation process does not detect any defect the car may move to the next phase. If that is not the case, then, the correspondent actions can be applied at once without creating any delays or bubbles in the process line, which is always an undesirable and costly event. These principles are usable in many other different fields. The glass, jewelry, paint and textile industries have obvious interests because colors are a direct way to evaluate the progress of the different production steps and final product design and quality. The Figure 15 shows a block diagram for a setup to perform color evaluation in the paint.

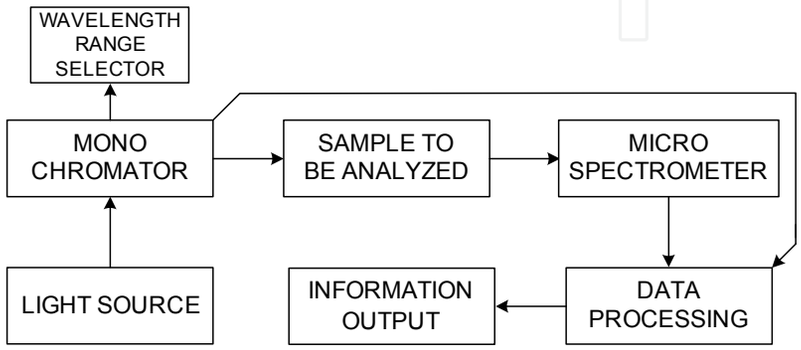


**Figure 15.** Color evaluation setup.

A light source projecting the full visible spectrum is narrowed down by a monochromator to set the desired wavelength range. Then, the selected spectrum is transmitted through the sample and the output light is recorded and analyzed by a photodetector and adequate software. In the following step, the resulting light is compared with the known selected light reference for improved resolution and sample characterization. By discriminating the difference between these two colors, a more accurate reading is obtained and a specific color pigment can be evaluated, investigated and discriminated. To finish with an example, it is possible to observe a photography showing a microspectrometer made in silicon for analysing the visible wavelength in the Figure 16. A detailed discussion about microspectrometers can be found in (Carmo J. P. et al., 2012a) and in (Wolffenbuttel R. F., 2005).

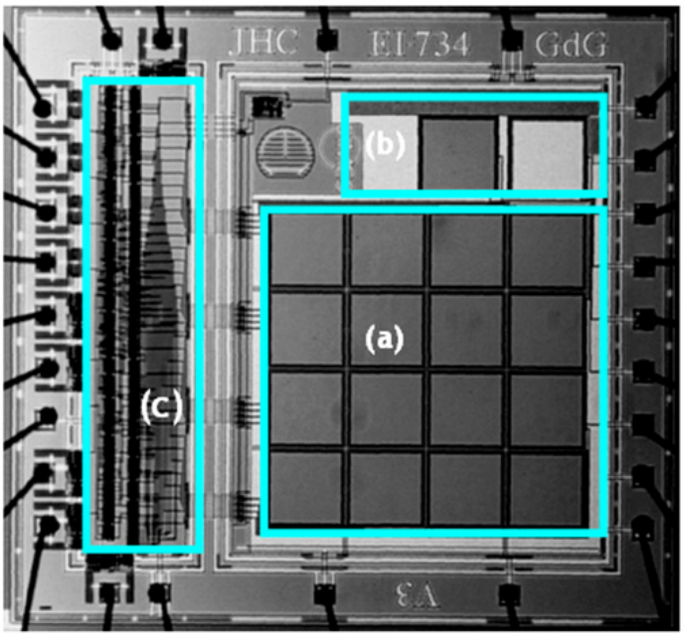


**Figure 16.** Photograph of a prototype of an array type microspectrometer composed by 16 channels, each one with a CMOS photodiode with a Fabry Perot etalon mounted on top. Three main subsystem blocks can be identified in the photograph: (a) array of 16 Fabry Perot mounted above 16 photodiodes, (b) dark current reduction, and (c) electronics for readout and signal processing (analog to digital conversion and amplification) and a serial bus for communicating with external devices (Carmo J. P. *et al*, 2012a). Reproduced with authorization of Elsevier Science.

## 5. Conclusions and further directos of research

This chapter presented optic techniques for analysing defects on vehicles. However, and given the importance of the vehicular industry in the world, the research doesn't finishes with one or other technique. To conclude this chapter it is important to reinforce the need of renewable power sources for reducing the greenhouse gas emissions to the atmosphere (Bell L. E., 2008) and to reduce the dependence of fossil fuel combustion sources (Vining C. B., 2008). The current research on production methods for obtaining the next generation algae biofuels is winning support as an even more sustainable alternative to fossil fuel sources (Savage N., 2011). However and despite the claim of experts to promote this upcoming

power source to be a sustainable energy, the biofuels don't solve the problem of greenhouse emissions (Wisner R., 2009) and is a threat to forests and agricultural fields (Hudiburg T. W. *et al*., 2011). Moreover, oils can't be yet produced at large scale from algae and at the same time further/though research in genetics must be done in order to engineer synthetic microorganisms for excreting the desired hydrocarbons (Biello D., 2011). The demand for combining vehicles with renewable power is even more evident when locking the hybrid vehicles available on roads (Boulanger A. G. *et al*., 2011) or the forthcoming generation of new plug¬ in vehicles that use the grid power to charge their lithium ion battery packs for powering their electric traction motors (Voelcker J., 2011). However and despite the availability of these type of vehicles, these is still much to do at the both the electronics (Cao J. *et al*., 2011) and batteries level (Kularatna N., 2011). In this sequence of ideas, it is still possible to provide cleaner forms of energy from vehicles based on internal combustion of oil derivatives. The heat released from the vehicle's engine can be scavenged using solid state thermoelectric generators (TEGs) based in the Seebeck effect for generating electricity in a process known as energy harvesting (Carmo J. P. *et al*., 2010). These TEGs characterizes for a few number of useful features, such as silent operation and without moving parts in its constitution (DiSalvio F. J., 1999). These features are behind the successful use by NASA of radioisotope TEGs (RTGs) for more than three decades of operation in deep space probes (Wolverton M., 2008) and are now under study for application in vehicles (Snyder G. J., 2008).

## Author details

J. P. Carmo
*University of Minho, Department of Industrial Electronics, Guimarães, Portugal*

J. E. Ribeiro
*Polytechnic Institute of Bragança, Department of Mechanical Technology, Bragança, Portugal*

## 6. References

Antunes, P., Varum, H., and André, P. (2011). Uniaxial fiber Bragg grating accelerometer system with temperature and cross axis insensitivity", *Measurement*, 44(*1*): 1-5.

Arregui, F. J., Matias, I. R., Cooper, K. L., and Claus, R. O. (2002). Simultaneous measurement of humidity and temperature by combining a reflective intensity-based optical fiber sensor and a fiber bragg grating, *IEEE Sensors Journal*, 2(*5*): 482-487.

Beard, P. C., and Mills, T. M. (1996). Extrinsic optical-fiber ultrasound sensor using a thin polymer film as a low-finesse Fabry-Perot interferometer, *Applied Optics*, 35(*4*): 663-675.

Beidermann, K., and Ek, L. (1975). A recording and display system for hologram interferometry with low resolution imaging devices, *Journal Physics E: Scientific Intruments*, 8(*7*): 571-574.

Bell, L. E. (2008). Cooling, heating, generating power, and recovering waste heat with thermoelectric systems, *Science*, 321: 1457-1462.

Biello, D. (2011). The false promise of biofuels, *Scientific American*, 305: 58-65.

Bifano, T. (2011). MEMS deformable mirrors, *Nature Photonics*, 5: 21-23.

Boerkamp, M., Lamb, D. W., and Lye, P. G. (2007) Using an intrinsic, exposed core, optical fibre sensor to quantify chemical scale formation, *Journal of Physics: Conference Series*, 76(*1*): 1-7. Institute of Physics Paper 012016.

Boulanger, A. G., Chu, A. C., Maxx, S., and Waltz, D. L. (2011). Vehicle electrification:status and issues, *Proceedings of the IEEE*, 99(*6*): 1116-1138.

Bruck, A., McNeil, R., Sutton, M., and Peters, H. (1989). Digital image correlation using Newton-Raphson method of partial differential correction, *Experimental Mechanics*, 29: 261-267.

Butters, J., and Leendertz, J. (1971). Holographic and video techniques applied to engineering measurement, Journal Measurement and Control, 12(4): 349-354.

Butters, N., Jones, R. C., and Wykes, C. (1975). Electronic speckle pattern interferometry in speckle metrology, *Springer-Verlag*, *New York*: 111-157.

Cao, J., and Emadi, A. (2011). Batteries need electronics, *Industrial Electronics Magazine*, 5(*1*): 27-35.

Carmo, J. P., Goncalves, L. M., and Correia, J. H. (2010). Thermoelectric microconverter for energy harvesting systems, IEEE Transactions on Industrial Electronics, 57(3): 861-867.

Carmo, J. P., Rocha, R. P., Bartek, M., de Graaf, G., Wolffenbuttel, R. F., and Correia, J. H. (2012a). A review of visible-range Fabry-Perot microspectrometers in silicon for the industry, *Optics & Laser Technology*, Accepted: 1–9.

Carmo, J. P., Silva, A. F., Rocha, R. P., and Correia, J. H. (2012b). Application of fiber Bragg gratings to wearable garments, *IEEE Sensors Journal*, 12(*1*): 261-266.

Chen, F., Brown, G. M., and Song, M. (2000). Overview of three-dimensional shape measurement using optical methods, Optical Engineering, 39(1): 10-22.

Chen, L., and Smith, P. (2000). Demonstration of incoherent wavelength-encoding/time-spreading optical CDMA using chirped moire gratings, *IEEE Photonics Technology Letters*, 12(*9*), 1281-1283.

Cheng, P., Kwak, S., and Choi, J. (2008). ESPI combined with hole drilling method to evaluate heat treatment induced residual stresses, Proceedings of the SPIE Fourth International Symposium on Precision Mechanical Measurements.

Cloud, G. (1998). *Optical methods of engineering analysis*, Cambridge University Press.

Creath, K. (1994). *Phase-shifting holographic interferometry*, Holographic Interferometry, Principles and Methods, Springer, Berlin, Ch. 5: 109-150.

Creath, K., and Schmit, J. (1996). N-point spatial phase-measurement techniques for non-destructive testing, *Optics and Lasers in Engineering*, 24: 365-379.

Denselight (2012). Denselight Semiconductors. Online and visited last time on 15th April 2012: http://www.denselight.com.

DiSalvo, F. J. (1999). Thermoelectric cooling and power generation, *Science*, 285: 703-706.

FiberSensing (2012). Online and visited last time on 15th April 2012: http://www.fibersensing.com.

Gabor, D. (1948). A new microscopic principle, *Nature*, 161(*3*): 777-778.

Gåsvik, K. J. (2002). *Optical metrology*, Third Edition, John Wiley & Sons Ltd, England.

Gu, X., Guan, L., He, Y., Zhang, H. B., and Herman, P. R. (2006). High-strength fiber bragg gratings for a temperature-sensing array, *IEEE Sensors Journal*, 6(*3*): 668-671.

Hill, K. O., and Meltz, G. (1997). Fiber Bragg grating technology fundamentals and overview, *IEEE Journal of Lightwave Technology*, 15(*8*): 1263-1276.

Hu, T., Ranson, W., Sutton, M., and Peters, W. (1985). Application of digital image correlation techniques to experimental mechanics, *Experimental Mechanics*, 25: 232-244.

Huang, P. S., and Zhang, S. (2006). Fast three-step phase shifting algorithm, *Applied Optics*, 45(*21*): 5086-5091.

Hudiburg, T. W., Law, B. E., Wirth, C., and Luyssaert, S. (2011). Regional carbon dioxide implications of forest bioenergy production, *Nature Climate Change*, 1: 419-423.

Hung, Y., and Taylor, C. (1973). A tool for measurement of derivatives of surface displacement, *Proceedings of the Society of Photo-Optical Instrumentation Engineering (SPIE)*, 41: 169-75.

Ibsen (2012). Ibsen photonics. Online and visited last time on 15th April 2012: http://www.ibsen.dk.

James, M. R., and Lu, J. (1996). *Handbook of measurement of residual stresses*, The Fairmont Press Inc., United States.

Jones, R., and Leendertz, J. A. (1974). Elastic constant and strain measurement using a three beam speckle pattern interferometer, *Journal of Physics E: Scientific Instruments*, 7(*8*): 653-657.

Jones, R., and Leendertz, J. A. (1974). Elastic constant and strain measurement using a three beam speckle pattern interferometer, *Journal Physics E: Scientific Intruments*, 7(8): 653-657.

Kersey, A. D., Davis, M. A., Patrick, H. J., LeBlanc, M., Koo, K. P., Askins, C. G., Putnum, M. A., and Friebele, E. J. (1997). Fiber grating sensors, *IEEE Journal of Lightwave Technology*, 15(*8*): 1442-1463.

Kong, S. H., Wijngaards, D. D. L., and Wolffenbuttel, R. F. (2001). Infrared micro-spectrometer based on a diffraction grating, *Sensors and Actuators A*: *Physical Sensors*, 92(*1-3*): 88-95.

Kularatna, N. (2011). Rechargeable batteries and their management, *IEEE Instrumentation & Measurement Magazine*, 14(*2*): 20-33.

Kung, P. (2009). Condition monitoring solutions for the wind turbines, Proceedings of the Canadian Machinery Vibration Association Seminar, Vancouver, Canada.

Lachheb, H., Puzenat, E., Houas, A., Ksibi, M., Elaloui, E., Guillard, C., Herrmann, J.-M. (2002). Photocatalytic degradation of various types of dyes (Alizarin S, Crocein Orange G, Methyl Red, Congo Red, Methylene Blue) in water by UV-irradiated titania, *Applied Catalysis B: Environmental*, 39: 75-90.

Lamé, M. G. (1852). *Leçons sur la théorie mathématique de l'élasticité des corps solids*, bachelier, Paris.

Leendertz, J. A., and Butters, J. N. (1973). An image-shearing speckle-pattern interferometer for measuring bending moments, *Journal of Physics E: Scientific Instruments*, 6(*11*): 1107-1110.

Lindblom, P., Meinander, M., and Olsson, T. (1990). Spectroscopy with the MEGA spectrometer, a very high resolution grating spectrometer, *Review of Scientific Instruments*, 61(*10*): 2546-2548.

Ling, H. Y., Lau, K. T., Cheng, L., and Jin, W. (2006). Viability of using an embedded FBG sensor in a composite structure for dynamic strain, *Measurement*, 39(*4*):328-334.

Lökberg, O. (1985). Electronic speckle pattern interferometry, *Physics in Technology*, 11: 16-22.

Lökberg, O., and Högmoen, K. (1976). Use of modulated reference wave in electronic speckle pattern interferometry, *Journal of Physics E: Scientific Instruments*, 9(*10*): 847-851.

Macovsky, A., Ramsey, S., and Shaeder, L. (1971). Time-laps interferometry and countering using television system, *Applied Optics*, 10: 2722-2727.

Marcellierl, H., Vescovo, P., Varchon, D., Vacher, P., Humbert, P. (2001). Optical analysis of displacement and strain fields on human skin, *Skin Research and Technology*, 7(*4*): 246-253.

Orr, P., and Niewczas, P. (2010). An optical fiber system design enabling simultaneous point measurement of magnetic field strength and temperature using low-birefringence FBGs, *Sensors and Actuators A*: *Physical Sensors*, 163(*1*): 68-74.

Peng, B. J., Zhao, Y., Yang, J., and Zhao, M. (2005). Pressure sensor based on a free elastic cylinder and birefringence effect on an FBG with temperature-compensation, *Measurement*, 38(*2*): 176-180.

Post, D., Han, B., and Ifju, P. (1994). High sensitivity moiré: experimental analysis for mechanics and materials, *Springer-Verlag*, New York.

Powell, R. L., and Stetson, K. A. (1965). Interferometric vibration analysis by wavefront reconstruction, *Journal of Optics Society of America*, l55(*12*): 1593-1598.

Rayleigh, L. (1874). On the manufacture and theory of diffraction gratings, *Philosophical Magazine*, 47(*310*): 81-93 & 193-205.

Ribeiro, J. E. (2006). *Caracterização experimental e numérica de campos de tensões residuais provocadas por processos de fabrico*, PhD Thesis, Faculdade de Engenharia da Universidade do Porto. *In Portuguese*.

Ribeiro, J., Monteiro, J., Lopes, and Vaz, M. (2011). Moiré interferometry assessment of residual stress variation in depth on a shot peened surface, *Journal of Strain: An International Journal for Experimental Mechanics*, 47: e542-e550.

Ribeiro, J., Monteiro, J., Vaz, M., and Lopes, H. (2009). Measurement of residual stresses with optical techniques, *Journal of Strain: An International Journal for Experimental Mechanics*, 45: 123-130.

Richter-Trummer, V., Moreira, P., Ribeiro, J., and Castro, P. (2011). The contour method for residual stress determination applied to an AA6082-T6 friction stir butt weld, *Materials Science Forum*, 681: 177-181.

Robinson, D. W., and Reid, G. T. (1993). *Interferogram analysis*, Ch. 5: 141-193, Ch. 4: 94-140, Ch. 6: 194-229. Institute of Physics (IOP), Bristol, 1993.

Rocha, R. P., Silva, A. F., Carmo, J. P., and Correia, J. H. (2011). FBG Sensor for measuring and recording the knee joint movement during gait, Proceedings of the 33rd Annual International Conference of the IEEE Engineering in Medicine and Biology Society (EMBC '11), Boston, Massachusetts, USA.

Saeki, Y., and Emura, T. (2002). Technical progresses for PVC production, *Progress in Polymer Science*, 27(*10*): 2055-2131.

Savage, N. (2011). Algae: the scum solution, *Nature*, 474: S15-S16.

Shang, H., and Gao, J. (2009). Theories and industrial applications of optical interferometric NDT techniques: a review, *Insight*, 51(*5*): 240-251.

Silva, A. F., Carmo, J. P., Mendes, P. M., and Correia, J. H. (2011). Simultaneous cardiac and respiratory frequency measurement based on a single fiber Bragg grating sensor, *Measurement Science and Technology*, 22(*7*): 1-5. Institute of Physics Paper 075801.

Silva, A. F., Goncalves, A. F., Ferreira, L. A., Araujo, F. M., Mendes, P. M., and Correia, J. H. (2011). A Smart skin PVC foil based on FBG sensors for monitoring strain and temperature, *IEEE Transactions on Industrial Electronics*, 58(*7*): 2728-2735.

Silva, A. F., Goncalves, A. F., Ferreira, L. A., Araujo, F. M., Mendes, P. M., and Correia, J. H. (2010). PVC smart sensing foil for advanced strain measurements, *IEEE Sensors Journal*, 10(*6*): 1149-1155.

Silva, A. F., Gonçalves, A. F., Mendes, P. M., and Correia, J. H. (2012). PVC formulation study for the manufacturing of a skin smart structure based in optical fiber elements, *Journal Polymers for Advanced Technologies*, *Wiley Publisher*, 23(*2*), 220-227.

Snyder, G. J. (2008). Small thermoelectric generators, *The Electrochemical Society Interface*, 17(*3*): 54-56.

Sutton, M. A., Cheng, Q., Peters, H., Chao, J., and McNeill, R. (1986). Application of an optimized digital correlation method to planar deformation analysis, *Image and Vision Computing*, 4: 143-151.

Sutton, M. A., McNeill, R., Jang, J., and Babai, M. (1988). Effects of subpixel image restoration on digital correlation error, *Journal of Optical Engineering*, 27: 870-877.

Sutton, M. A., Orteu, J., and Schreier, H. W. (2009). Image correlation for shape, motion and deformation measurements, *Springer Science+Business Media*, New York.

Sutton, M. A., Turner, L., Bruck, A., and Chae, A. (1991). Full-field representation of discretely sampled surface deformation for displacement and strain analysis, *Experimental Mechanics*, 31: 168-177.

Sutton, M. A., Wolters, J., Peters, H., Ranson, F., and McNeil, R. (1983). Determination of displacements using an improved digital correlation method, *Image and Vision Computating*, 1: 133-139.

Svanbro, A. (2005). *Speckle interferometry and correlation applied to large-displacement fields*, PhD Thesis, Luleå University of Technology.

Takasaki, H. (1970). Moiré topography, *Applied Optics*, 9(*6*): pp 1467-1472.

ThorLabs (2012). Thorlabs GmbH, Germany. Online and visited last time on 15th April 2012: http://www.thorlabs.de.

Vining, C. B. (2008). Desperately seeking silicon, *Nature*, 451: 132-133.

Voelcker, J. (2011). One million plugin cars by 2015?, *IEEE Spectrum INT* (*International Edition*): 9-11.

Wang, Q., Rajan, G., Wang, P., and Farrell, G. (2007). Macrobending fiber loss filter, ratiometricwavelength measurement and application, *Measurement Science Technology*, 18(*10*): 3082-3088.

Wei, C. L., Lai, C. C., Liu, S. Y., Chung, W. H., Ho, T. K., Ho, S. L., McCusker, A. Kam, J., and Lee, K. Y. (2010). A fiber bragg grating sensor system for train axle counting, *IEEE Sensors Journal*, 10(*12*): 1905-1912.

Wisner, R. (2009). Biofuels and greenhouse gas emissions on a collision course, *Oil Mill Gazetter*, 114: 2-20.

Wolffenbuttel, R. F. (2005). MEMS-based optical mini and microspectrometers for the visible and infrared spectral range, *Journal of Micromechanics and Microengineering* 15(*7*): S145-S152.

Wolverton, M. (2008). Stirling in deep space: to cut back on radioisotope fuel, NASA goes back 200 year, *Scientific American*, 298:22.

Wronkowski, L. (1995). Diffraction model of an optoelectronic displacement measuring transducer, *Optics & Laser Technology*, 27(*2*):81–89.

Xie, F., Chen, Z., and Ren, J. (2009). Stabilisation of an optical fiber Michelson interferometer measurement system using a simple feedback circuit", *Measurement*, 42(*9*): 1335-1340.

Xie, F., Chen, Z., and Ren, J. (2009). Stabilisation of an optical fiber Michelson interferometer measurement system using a simple feedback circuit, *Measurement*, 42(*9*): 1335-1340.

Xie, H., Shang, H., Dai, F., Li, B., and Xing, Y. (2004). Phase shifting SEM moiré method, *Optics & Laser Technology*, 36(*4*), 291–297.

Yao, S.-K., and Asawa, C. (1983). Fiber optical intensity sensors, *IEEE Selected Areas in Communications*, 1(*3*): 562-575.

Zhang, S. (2010). Recent progresses on real-time 3D shape measurement using digital fringe projection techniques, *Optics and Lasers in Engineering*, 48: 149-158.

Zhang, Y., Ghosal, S., Casstevens, M, and Burzynski, R. (1995). Bifunctional chromophore for photorefractive applications, *Applied Physics Letters*, 66(*3*): 256-258.

Zhao, Y., Zhao, Y., and Zhao, M. (2005). Novel force sensor based on a couple of fiber Bragg gratings, *Measurement*, 38(*1*): 30-33.

Zhou, W., Dong, X., Ni, K., Chan, C. C., and Shum, P. (2010) Temperature insensitive accelerometer based on a strain chirped FBG, *Sensors and Actuators A: Physical Sensors*, 157(*1*): 15-18.